Hindawi
Geofluids
Volume 2022, Article ID 9142345, 12 pages
https://doi.org/10.1155/2022/9142345

Research Article

Similarity Model Test of Coal Mining under Ordovician Limestone Nappe Aquifer

Chengcheng Chu

Department of Earth and Environment, Anhui University of Science and Technology, Huainan, Anhui 232001, China

Correspondence should be addressed to Chengcheng Chu; 2017006@aust.edu.cn

Received 8 February 2022; Accepted 1 March 2022; Published 17 March 2022

Academic Editor: Di Feng

Ordovician limestone in North China coalfield has the characteristics of karst fissure development and strong water yield. Coal mines in North China have been threatened by Ordovician limestone water for a long time. Taking the mining of 3_2 coal seam in the first eastern mining area of Qianyingzi coal mine in Anhui Province in China as the engineering geological prototype, this paper uses the self-developed fluid solid coupling similarity model test device to carry out the similarity model test of overburden stress and pore water pressure response of coal mining under Ordovician limestone nappe aquifer. Based on the variation law of pore water pressure and overburden stress in a stope, it can be seen that the variation law of pore water pressure in confined aquifer is jointly affected by two factors: the vertical distance between the monitoring point and coal seam and the horizontal distance between the monitoring point and DF200 fault. According to the analysis of experimental results, the maximum height of a water flowing fracture zone in the stope is fifteen times the mining thickness. Compared with the theoretical calculation results of empirical formula, the coupling effect of seepage field and stress field and the geological structure characteristics of the stope promote the development of a water flowing fracture zone. The research results of this paper have important theoretical and practical significance not only for the safe mining of Qianyingzi coal mine but also for the safe mining of the coal mine facing the double threat of roof Ordovician limestone confined aquifer and reverse fault.

1. Introduction

In recent years, with the accelerated pace of national energy transformation, continuous optimization of energy structure, and slowdown of coal demand, China's resource endowment characteristics of lack of gas, less oil, and relatively rich coal determine that the dominant position of coal as energy will not change for a long time in the future [1, 2]. According to the data of the National Bureau of Statistics in 2019, coal accounts for 68.8% of the primary energy production and 57.7% of the consumption structure, respectively. In China, coal resources have the characteristics of unbalanced regional distribution of more in the west and less in the east and rich in the north and poor in the south, which is inversely distributed with the developed degree of regional economic distribution. Therefore, North China coalfield plays an important role in the distribution pattern of coal resources at this stage with its rich coal resource reserves and good natural geographical location; especially under the action of thrust nappe structure in the strong compression deformation area in the southwest, the potential of deep coal resources is great [3, 4]. Thrust nappe structure is a large-scale and low-angle thrust fault. The hanging wall of the fault migrates from a distance, which is called external system or nappe, and the footwall of the fault is called in situ system. As the whole crust of North China coalfield uplifted at the end of the middle Ordovician and suffered weathering and denudation for a long time until it fell again and accepted settlement in the middle Carboniferous, the Ordovician limestone has the characteristics of karst fissure development and strong water yield. The coal mining in North China, especially in Hebei, Henan, Shandong, and Anhui provinces, has been greatly threatened by Ordovician limestone water for a long time [5–18]. Strengthening the research on coal mining under Ordovician limestone nappe aquifer and tapping deep resource potential is of great

practical significance to alleviate the uneven distribution of coal resources and solve the contradiction between energy supply and demand in some areas.

Similarity model test is an important technical means for research in the field of engineering geology. Compared with theoretical methods and numerical simulation methods, physical simulation can qualitatively or quantitatively reflect the construction technology, load action mode, and time effect of complex projects and can study the whole process of engineering stress, from elasticity to plasticity to failure mode after ultimate load. At present, China's research on coal mining under aquifer mainly focuses on coal mining under loose aquifer [16–29]. Some scholars have conducted in-depth research on coal mining under loose aquifer by using the similarity model test. Li et al. [30] proposed that the stress field and geophysical field before water inrush in the coal seam mining under the loose aquifer have obvious precursory characteristics by monitoring the variation characteristics and abnormal signals of the stress field, displacement field, seepage field, temperature field, and electric field and acoustic emission information of the surrounding rock of the aquiclude in the whole process. Sui and Dong [31] used centrifugal model test to study the variation law of pore water pressure in coal seam mined out area under loose aquifer and clay layer above coal pillar. The test shows that the variation of pore water pressure in confined aquifer caused by mining is closely related to coal seam mining progress and roof periodic pressure; the pore water pressure in the aquifer above the coal pillar generally increases first and then decreases. The change of pore water pressure in the aquifer above the working face is related to the mining location. Once the water sand inrush is formed, the pore water pressure of the aquifer decreases sharply and forms an instantaneous negative pressure. The test results provide a precursory information source for the prediction and prevention of sand break disaster in mining near loose aquifer. Du et al. [32] applied the distributed optical fiber sensing technology to the similarity model test of shallow coal seam mining, proposed the quantitative index of the coupling relationship between the sensing optical fiber and the mining rock mass, and reasonably divided the vertical zoning area of overburden caused by mining, which provided a new idea for the detection of the development height of a water flowing fracture zone.

Different from the loose aquifer, the roof water inrush mechanism and overburden movement and deformation characteristics of coal mining under limestone (Ordovician limestone and Cambrian limestone) aquifer are often coupled with faults. The existence of faults makes the geological conditions of the stope more complex. Taking the mining of 3_2 coal seam in the first eastern mining area of Qianyingzi coal mine in Anhui Province in China as the engineering geological prototype, this paper uses the self-developed fluid solid coupling similarity model test device to carry out the similarity model test of overburden stress and pore water pressure response of coal mining under Ordovician limestone nappe aquifer. The research results of this paper have important theoretical and practical significance not only for the safe mining of Qianyingzi coal mine but also for the safe mining of coal mine facing the double threat of roof Ordovician limestone confined aquifer and reverse fault.

2. Engineering Geological and Hydrogeological Conditions of the Study Area

The study area is the first eastern mining area of Qianyingzi coal mine in Anhui Province in China. Qianyingzi coal mine is the stratigraphic type of Huaibei coalfield, belonging to the North China stratigraphic category. The first eastern mining area is located in the southeast of Qianyingzi coal mine. The mining depth of 3_2 coal seam in the first eastern mining area of Qianyingzi coal mine is -280~-650 m; the average thickness of 3_2 coal seam is 3.3 m. DF200 fault has a dip angle of about 45 degrees and is rich in water and weak in water conductivity. The strata in the study area are Ordovician, Carboniferous, Permian, Neogene, and Quaternary from the bottom to the top. The Permian Shanxi Formation, lower Shihezi Formation, and upper Shihezi Formation are the main coal-bearing strata. The aquifers in the mining area include Cenozoic unconsolidated aquifer, Permian sandstone fractured aquifer, and Ordovician limestone fractured aquifer. There are stable water barriers between the first, the second, and the third aquifers of Cenozoic. Generally, there is no hydraulic connection between these aquifers. The fourth aquifer has a certain hydraulic connection with sandstone fractured aquifer in some places. Permian sandstone fractured aquifer has poor connectivity and weak water yield. The results of unsteady flow pumping test of group holes show that the Ordovician limestone aquifer has a hydraulic connection with the surrounding aquifer and is a medium water-rich aquifer. DF200 fault makes Ordovician limestone directly push over the roof of 3_2 coal seam, forming a limestone nappe aquifer. Therefore, 3_2 coal seam mining is threatened by both DF200 fault and Ordovician limestone aquifer.

According to the drilling data, the overburden of 3_2 coal seam is mainly interbedded with sandstone and mudstone. The thickness of roof mudstone is small, and most of them belong to soft rock with poor stability. Sandstone is a medium hard rock stratum with hard and dense rock, high compressive strength, and good stability. The mining hydrogeological and engineering geological model of the study area is shown in Figure 1.

3. Test Scheme

The fluid-solid coupling similarity model takes the engineering geological model -550 m level as the bottom interface and 0 m level as the top interface. The scale between the model and the prototype is 1 : 500. The length, width, and height of the model are 180 cm, 15 cm, and 110 cm, respectively. The coal seam thickness in the model is 1 cm, which is equivalent to the actual mining thickness of 5 m. As shown in Table 1, in the similarity model test, the water-resisting layer is made of sand and talc as aggregate, paraffin as binder, and vaseline and tung oil as modified water material.

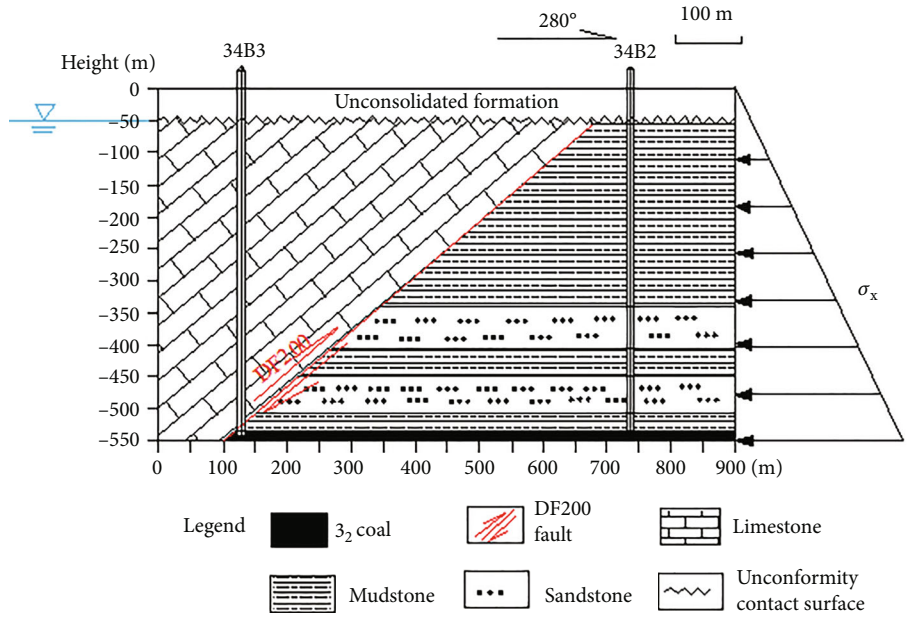

Figure 1: Mining hydrogeological and engineering geological model in the study area.

Table 1: Material mixture for the water-resisting layer in a physical model.

Lithology	Film forming temperature (°C)	Particle size (mm)	Mass ratio of sand and talc	Paraffin (%)	Vaseline (%)	Tung oil (%)
Mudstone	40	0.25-0.5	3 : 1	8	8	8
Sandstone	60	0.5-1	3 : 1	10	5	0

In the model test, mining starts from 40 cm away from the right boundary of the model. The mining direction is from right to left along the coal seam. Each mining step is 4 cm, with a total of 20 steps. In the model test, the mining distance is 80 cm, which is equivalent to the actual mining of 400 m.

3.1. Experimental Setup. The fluid-solid coupling similarity model test device is composed of model box, water supply system, stress monitoring system, water pressure monitoring system, and image acquisition system.

The stress monitoring system includes two parts: pressure sensor and data collector. The strain earth pressure box is selected as the sensor for stress monitoring, which has the characteristics of small volume, high sensitivity, good waterproof performance, dynamic acquisition, and long-term stability. The diameter of the sensor is 28 mm, and the thickness is 10 mm. The signal acquisition device of the sensor is dataTaker DT515 automatic data acquisition instrument.

The water pressure monitoring system consists of glass tubes with openings at both ends, glass tube fixed supports, connecting tubes, and embedded tubes. Through the connection of connecting tubes and embedded tubes, the glass tubes are connected with the water pressure monitoring points. The change of water head height in the glass tubes can directly reflect the change of pore water pressure at the monitoring points during the test process.

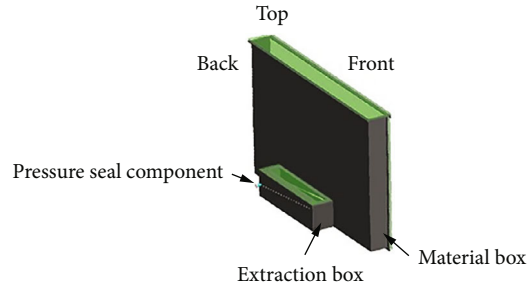

Figure 2: Diagram of model box.

The model box includes three parts: material box, extraction box, and pressure seal component (Figure 2). Among them, the pressure seal component is the key component of the model box, which can not only realize the requirements of step-by-step mining during coal seam excavation but also meet the sealing of the model box. The pressure seal component is composed of extraction plate, nut, screw sleeve, screw guide sleeve, and screw, as shown in Figure 3. The extraction plate is used to simulate coal seam mining. In the model test, the thickness of the extraction plate represents the thickness of the coal seam mined. The width of the extraction plate determines the distance of each mining step of the coal seam. Its design size is 15 cm long and 4 cm wide. According to the setting of mining steps of coal seam in the model test, 20 sets of pressure seal components are used in this test to realize step-by-step mining of coal seam.

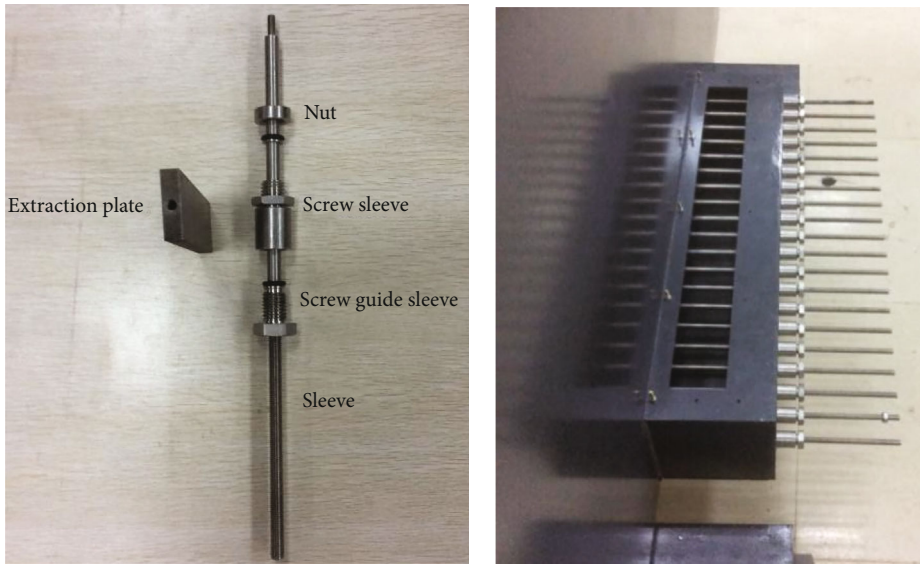

(a) Composition diagram (b) Assembly drawing

Figure 3: Picture of pressure seal component.

The material box is the space for laying similar materials and placing sensors. It is the main structure of the whole model box. The length, width, and height of the material box are 180 cm, 15 cm, and 110 cm, respectively. In order to meet the functional requirements of visibility and pressure resistance of the test device at the same time, the front and top of the box are made of acrylic plate, and the back, side, and bottom are made of steel plate. Meanwhile, in order to simulate the mining of coal seam, a gap with a horizontal length of 80 cm, an included angle of 6° with the horizontal direction, and a width of 1 cm is designed on the steel plate on the back of the box, as shown in Figure 4.

Figure 4: Picture of material box.

3.2. Layout of Monitoring Points

3.2.1. Layout of Stress Monitoring Points. As shown in Figure 5, 17 stress monitoring points are arranged in the model test. Among them, 4 monitoring points are located in the footwall of F18 fault, and the other 13 monitoring points are located between F18 fault and DF200 fault. Among the 13 monitoring points located between the two faults, No. 2, No. 7, No. 12, and No. 17 monitoring points are located in front of the goaf, and the rest are located above the goaf. Meanwhile, the monitoring points (No. 3 to No. 17) above the coal seam are located on three horizontal side lines parallel to the coal seam, and the vertical distances between the three side lines and the coal seam are 5.4 cm, 12 cm, and 15 cm, respectively.

3.2.2. Layout of Pore Water Pressure Monitoring Points. As shown in Figure 6, 16 pore water pressure monitoring points are arranged in the test. All pore water pressure monitoring points are located in the limestone aquifer above the coal seam. The heights of the four horizontal survey lines from the bottom boundary of the model are 23 cm, 28 cm, 32 cm, and 38 cm, respectively, and the distance between two adjacent survey points on the same horizontal survey line is 10 cm.

4. Analysis of Test Results

4.1. Overburden Stress Analysis. Figure 7 is the contour map of overburden stress change after the model is fully mined. In the figure, coordinate X represents the distance from the left boundary of the model, coordinate Y represents the distance from the bottom boundary of the model, and coordinate Z represents the change of stress value before and after model mining. It can be seen from the figure that

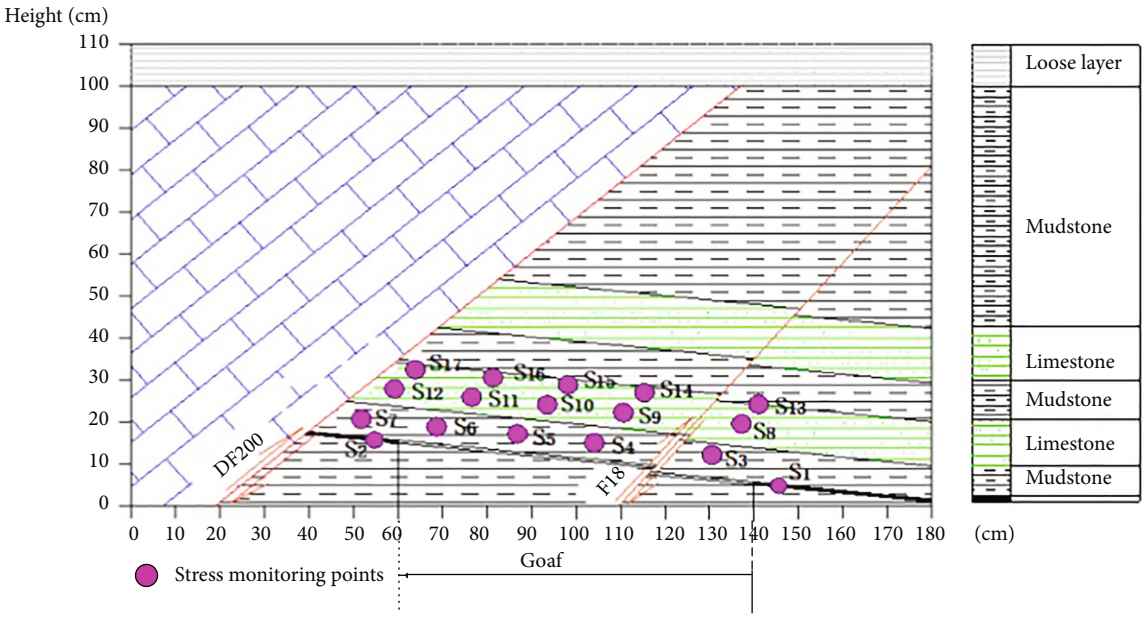

Figure 5: Stress monitoring layout.

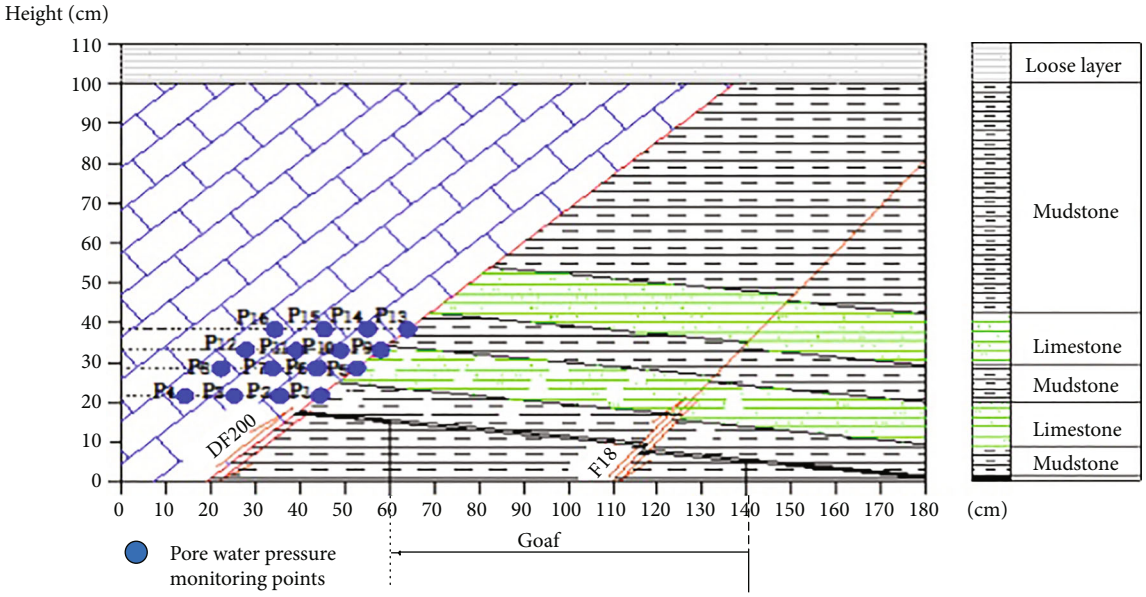

Figure 6: Distribution of pore water pressure monitoring points.

the stress unloading area above the goaf is centered on $x = 110$ cm in the horizontal direction and has obvious zoning characteristics to the left and right sides, which can be divided into a strong decompression area, weak decompression area, and transition area. Under simulated geological conditions, the zoning characteristics on both sides are asymmetric distribution. The average reduction range of internal stress in the strong decompression zone is 86.3%, that in the weak decompression zone is 51.8%, and that in the transition zone is 8.7%. If it continues to expand to both sides, the stress value will increase.

As shown in Figure 8, with the increase of mining distance, the main variation laws of stress values at No. 1~17 stress monitoring points are as follows:

(1) No. 1 and No. 2 monitoring points are located 5 cm in front of and behind the goaf, respectively. During the mining process of the model, the stress values of the two monitoring points fluctuate but generally show a trend of gradually increasing with the increase of mining distance

(2) Except for No. 7 and No. 12 monitoring points, other monitoring points of No. 3~16 monitoring

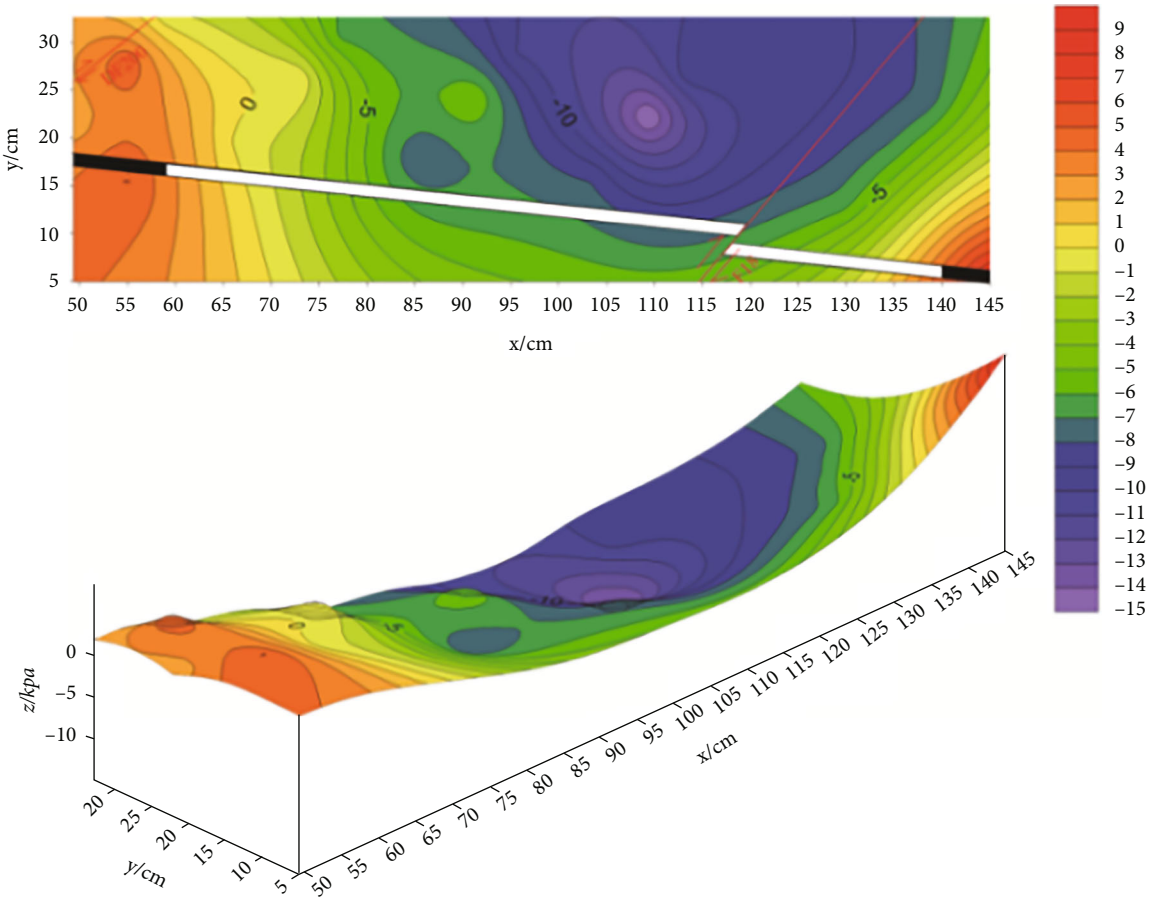

Figure 7: Contour map of overburden stress variation after mining totally (unit: kPa).

points are located above the goaf. After completed mining of the model, the stress value of these monitoring points decreases. Because cracks are generated first and then closed affected by the deformation of the upper rock stratum, the stress value of No. 8 and No. 13 monitoring points first decrease to 0 and then increase gradually during the model mining

(3) No. 7, No. 12, and No. 17 monitoring points are located above the coal seam and in front of the goaf. Meanwhile, No. 17 point is the nearest monitoring point to DF200 fault. The stress values of No. 7 and No. 12 monitoring points gradually increase with the increase of mining distance. However, due to the influence of fluid-solid coupling of the stope and DF200 fault, the stress value of No. 17 monitoring point decreases after complete mining

(4) After the model is fully mined, the stress ratio of 17 stress monitoring points is shown in Table 2. The stress ratio refers to the ratio of the stress value of the monitoring point after the model is fully mined to the initial stress value of the model before mining. By analyzing the variation law of overburden stress from the perspective of the position relationship between the monitoring point and the goaf, it can be concluded that:

(1) The stress increase of the No. 2 monitoring point is the largest, with a stress ratio of 1.8 and an increase of 80%. The stress ratio of the No. 1 monitoring point is 1.65, with a stress increase of 65%, indicating that the stress increase in front of the goaf is greater than that after the goaf

(2) The stress ratio of the No. 12 monitoring point is 1.45, with an increase of 45%; the stress ratio of the No. 7 monitoring point is 1.25, with an increase of 25%; the stress ratio of the No. 17 monitoring point is 0.92, with a decrease of 8%

(3) Among monitoring points of No. 3~No. 16 (except monitoring points of No. 7 and No. 12), the stress of the No. 14 monitoring point has the largest decrease, with a stress ratio of 0 and a decrease of 100%; the stress ratio of the No. 3 monitoring point is 0.04, with a stress decrease of 96%; the stress ratio of the No. 9 monitoring point is 0.09, with a stress decrease of 91%; and the stress ratio of the No. 15 monitoring point is 0.10, with a stress decrease of

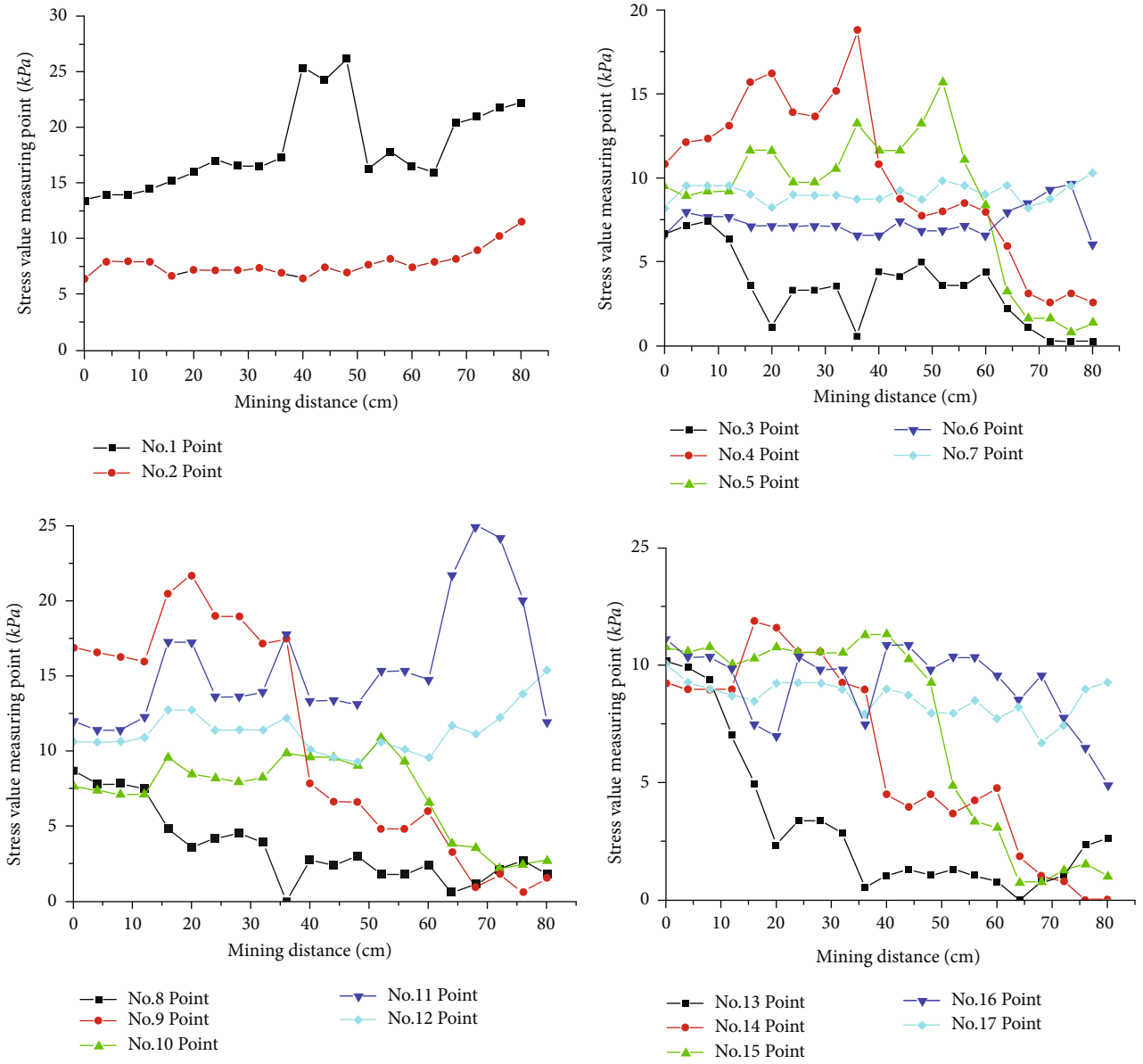

Figure 8: Dynamic change regularity of No. 1-17 stress monitoring points along with mining distance.

90%. Generally, the average decrease of the stress value of monitoring points above the goaf is 68.5%

In summary, the decrease of the lower wall stress value of F18 fault is larger than the decrease of the upper wall stress value of F18 fault. Along the direction of coal seam mining, the decrease of the stress value of the rock formation above the goaf shows a trend of decreasing first, increasing, and then decreasing. In the rock formation between the F18 fault and DF200 fault, the geodesic directions consisting of No. 5, No. 10, and No. 15 located in the middle of the mining area are the directions with the largest decrease in stress above the goaf.

Combined with the development characteristics of overlying rock fractures in the stope, the maximum height of the water flowing fracture zone is 75 m, and the ratio of the height of the water flowing fracture zone and the mining thickness is 15. Comparing the calculation results of empirical equation 1 and empirical equation 2 calculated from the height of the water flowing fracture zone of medium and hard roof strata in the procedures for coal pillar reservation and coal mining of buildings, water bodies, railways, and main roadways [29], the coupling effect of seepage field and stress field and the geological construction characteristics of the mining area have a promoting effect on the development of the water flowing fracture zone, as shown in Table 3.

4.2. Pore Water Pressure Analysis. The variation law of pore water pressure value of water pressure monitoring points with mining distance is shown in Figure 9. It can be seen

Table 2: Stress ratio of monitoring points.

Monitoring point position	Monitoring point number	Vertical distance from coal seam (cm)	Stress ratio of model after full mining and before mining
Behind the goaf	1	0	1.65
In front of the goaf	2	0	1.80
Above the goaf	3	5.4	0.04
	4	5.4	0.24
	5	5.4	0.14
	6	5.4	0.91
	8	12	0.21
	9	12	0.09
	10	12	0.36
	11	12	0.99
	13	15	0.26
	14	15	0
	15	15	0.10
	16	15	0.44
In front of the goaf	7	5.4	1.25
	12	12	1.45
	17	15	0.92

Table 3: Calculation value of development height of the water flowing fracture zone in the stope.

Number	Equation	The height of water flowing fracture zone (cm)	The ratio of the height of water flowing fracture zone and the mining thickness
Equation 1	$\left(100\sum M/1.6\sum M + 3.6\right) \pm 5.6$	37.5-48.7	7.5-9.7
Equation 2	$20\sqrt{\sum M} + 10$	54.72	10.9

Note: ΣM refers to the mining thickness.

that pore water pressure values of 16 water pressure monitoring points, which are located in front of the working face, are consistent with the trend of gradually increasing with mining distance and show a fluctuation relationship consistent with the change of roof stress in the stope. At the initial stage of model mining, the water pressure values of No.1~No.16 pore water pressure monitoring points do not change significantly. After the fourth mining step, the pore water pressure values of monitoring points begin to increase. With the continuous advancement of the working face, pore water pressure values gradually increase. After the tenth and seventeenth mining step, the pore water pressure values increase significantly. Compared with the variation law of roof stress in the stope, the roof stress value changes little at the initial stage of mining. After the fourth mining step, the stress values of No. 4 and No. 5 stress monitoring points closest to the front of the work increase significantly.

Figure 10 shows the growth rate of water pressure of No.1~No.16 pore water pressure monitoring points after the model is fully mined. It can be seen from the figure that the change of pore water pressure is related to two factors: the vertical height of the monitoring point from the coal seam roof and the horizontal distance between the monitoring point and DF200 fault.

From the perspective of the vertical distance between pore water pressure monitoring point and the coal seam roof, at different levels, the increase of pore water pressure at the monitoring point close to the coal seam roof is relatively large, and the change range of pore water pressure at the monitoring point far from the coal seam roof is relatively small. From the perspective of the horizontal distance between pore water pressure monitoring point and DF200 fault, at the same horizontal height, the pore water pressure value of the monitoring point close to DF200 fault increases greatly.

4.3. Linkage Response of Pore Water Pressure and Overburden Stress. Among pore water pressure monitoring points, No. 1, No. 5, No. 9, and No. 13 monitoring points are located on the DF200 fault. After the model is fully mined, the increase of pore water pressure values of above four monitoring points is 49%, 55%, 33%, and 26%, respectively. Among overburden stress monitoring points, No. 7,

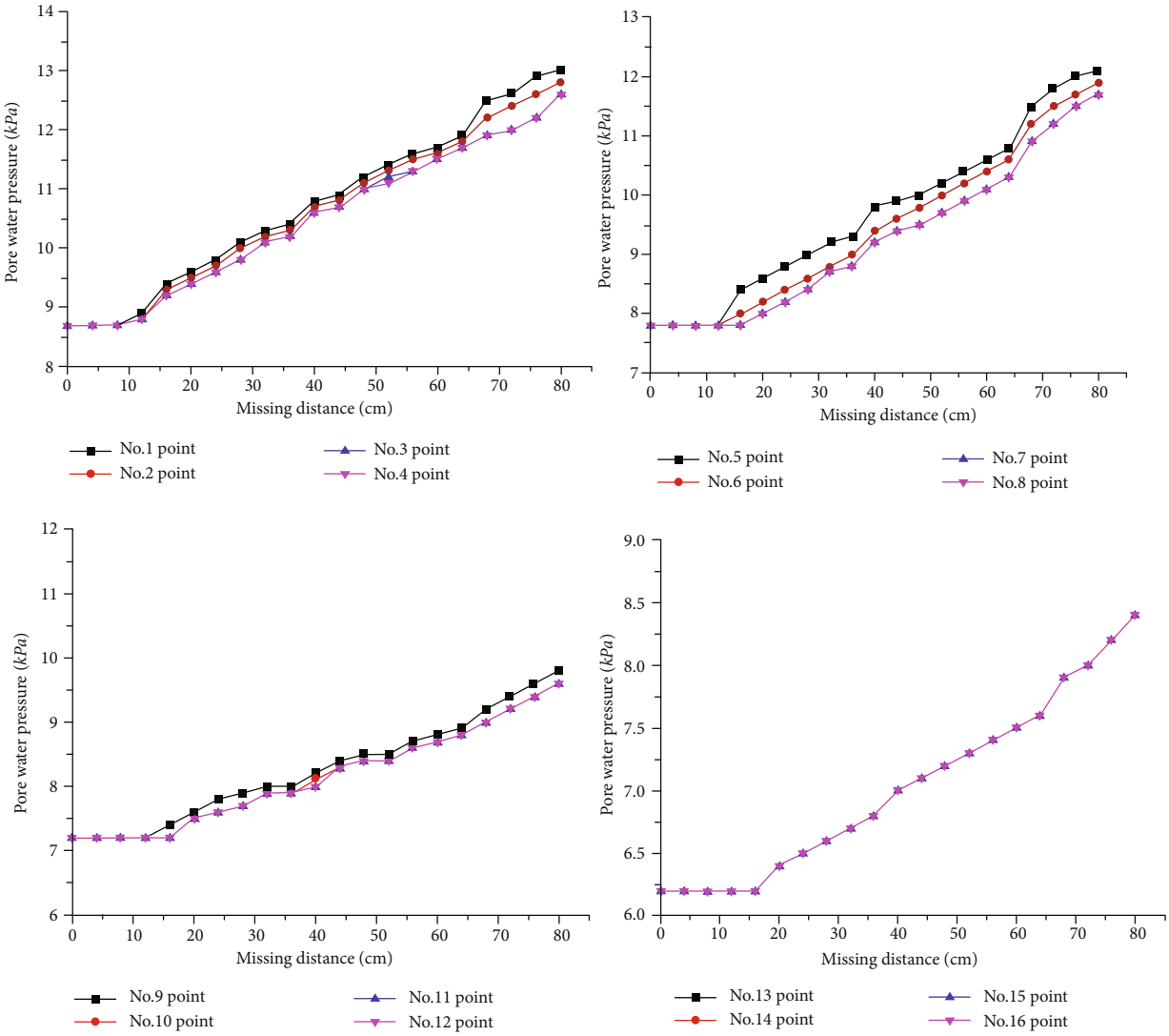

Figure 9: Law of pore water pressure with mining distance.

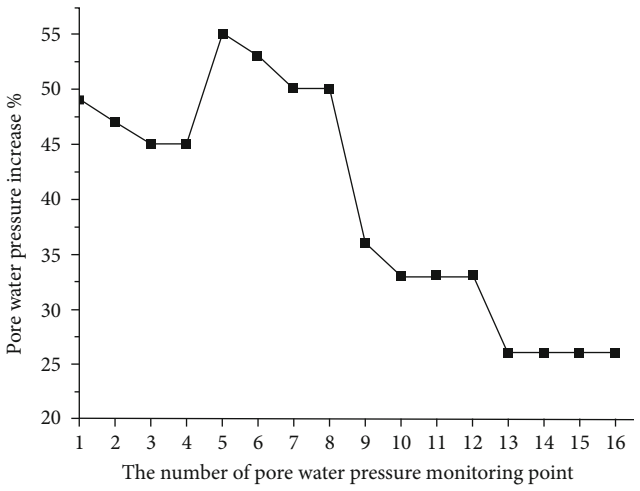

Figure 10: Growth rate of pore water pressure at monitoring points.

No. 12, and No. 17 are three stress monitoring points closest to the DF200 fault. In addition, the No. 7 stress monitoring point is close to the No. 1 pore water pressure monitoring point, No. 12 stress monitoring point is close to the No. 5 pore water pressure monitoring point, and the No. 17 stress monitoring point is close to the No. 9 pore water pressure monitoring point. By comprehensively analyzing the variation law of the water pressure value of pore water pressure monitoring point in confined aquifer and the stress value of overburden stress monitoring point, it can be seen that near the DF200 fault, the increase of the water pressure value of the No. 5 pore water pressure monitoring point is the largest, which is closest to the No. 12 stress monitoring point with the largest stress increase after the model is fully mined. There is a coupling effect between the seepage field and stress field.

As shown in Figure 11, combined with the data of the No. 1 pore water pressure monitoring point and No. 4 and No. 5 stress monitoring points, which are located above the middle of the goaf, the linkage response law of pore

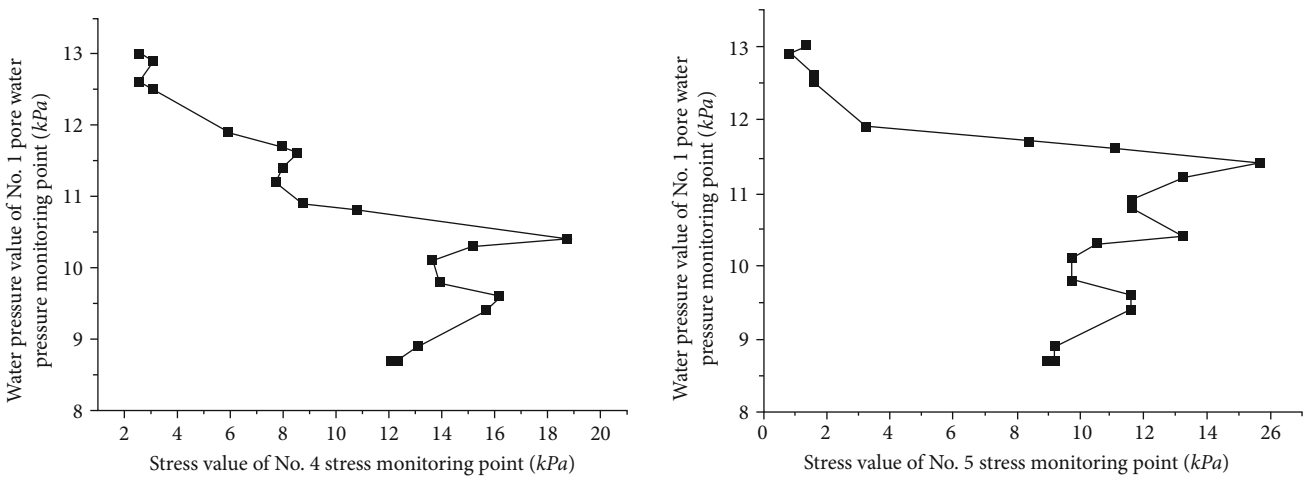

Figure 11: Connected effect between pore water pressure and overburden stress in the mining process.

water pressure and overburden stress during mining can be seen as follows:

(1) When the stress monitoring point is in front of the working face, the variation law of pore water pressure increases gradually with the increase of overburden stress, and the growth rate of pore water pressure is relatively stable

(2) When the working face passes below the stress monitoring point, the overburden stress decreases and the pore water pressure continues to increase until the model is completely mined without water inrush. In this process, the change law of pore water pressure is divided into two stages. The first stage is at the initial stage of stress unloading, overburden stress decreases rapidly, and pore water pressure increases slowly. In the second stage, when the working face passes a distance below the stress monitoring point, with the continuous advancement of the working face to the front aquifer, the change of overburden stress decreases, and the growth rate of pore water pressure increases rapidly

5. Conclusion

The research on overburden stress and water pressure response to mining under Ordovician limestone nappe aquifer is a new subject of coal mine safety production. Taking the mining of 3_2 coal seam in the first eastern mining area of Qianyingzi coal mine in Anhui Province in China as the engineering geological prototype, using the self-developed similarity model test device, this paper can fully consider the geological structure characteristics of the stope while meeting the simulation of the mining process of coal seam under confined aquifer and overcome the key technical problems of step-by-step mining of coal seam under sealed conditions; the fluid-solid coupling similarity model test of coal seam mining under Ordovician limestone nappe aquifer is carried out, focusing on the changes of overburden stress and water pressure of confined aquifer in the process of coal seam mining. The main conclusions are as follows:

(1) The stress unloading area above the goaf presents obvious zoning characteristics to the left and right sides in the horizontal direction, which can be divided into a strong decompression area, weak decompression area, and transition area. Under the simulated geological conditions, the zoning characteristics on both sides have asymmetric distribution. The average reduction range of internal stress in the strong decompression zone is 86.3%, that in the weak decompression zone is 51.8%, and that in the transition zone is 8.7%. If it continues to expand to both sides, the stress value will increase

(2) The maximum height of the water flowing fracture zone is 75 m in the stope, and the ratio of the height of the water flowing fracture zone and the mining thickness is 15. Combined with the lithology characteristics of the stope roof, the empirical formula 1 and empirical formula 2 for calculating the height of the water flowing fracture zone in the medium hard roof slate given in the procedures for coal pillar reservation and coal mining of buildings, water bodies, railways, and main roadways are used for calculation. The theoretical values of the development height of the water flowing fracture zone in the stope are 30.1~41.3 m and 44.6 m, and the ratio of the height of the water flowing fracture zone and the mining thickness is 7.5-10.7 and 10.9. It can be seen that the development height of the water flowing fracture zone in the stope is jointly affected by the coupling effect of stress field and seepage field and the characteristics of geological structure

(3) Pore water pressure monitoring points are located in front of the goaf, and there is no water inrush during the mining process of the model. The change law of pore water pressure generally increases with the increase of mining distance. The change law of pore

water pressure is affected by two factors: the vertical distance between the monitoring point and the coal seam and the horizontal distance between the monitoring point and DF200 fault. By comprehensively analyzing the variation law of the water pressure value of pore water pressure monitoring point in confined aquifer and the stress value of overburden stress monitoring point, it can be seen that near the DF200 fault, the increase of the water pressure value of the No. 5 pore water pressure monitoring point is the largest, which is closest to the No. 12 stress monitoring point with the largest stress increase after the model is fully mined. There is a coupling effect between the seepage field and stress field

Data Availability

The data supporting the findings of this study are available within the article and are available from the corresponding author on request.

Conflicts of Interest

The author declares that they have no conflicts of interest.

Acknowledgments

This work was supported by the Natural Science Foundation of Anhui Science and Technology Department of China under Grant No. 1908085QE248 and the Natural Science Foundation of Anhui Education Department of China under Grant No. KJ2018A0100.

References

[1] L. Yuan, "Research progress of mining response and disaster prevention and control in deep coal mines," *Journal of China Coal Society*, vol. 46, no. 3, pp. 716–725, 2021.

[2] L. Yuan, "Scientific conception of precision coal mining," *Journal of China Coal Society*, vol. 42, no. 1, pp. 1–7, 2017.

[3] A. O. Wei-hua, H. U. Wen-hui, Y. A. Yan-bin, and L. I. Hao, "Features and development potential of deep coal resources in the east of northern China," *Resources and industries*, vol. 14, no. 3, pp. 84–90, 2012.

[4] H. Lan, D. K. Chen, and D. B. Mao, "Current status of deep mining and disaster prevention in China," *Coal Science and Technology*, vol. 44, no. 1, pp. 39–46, 2016.

[5] T. C. Zhao, *Comprehensive Control Technology of Ordovician Limestone Water in North China*, Coal Industry Press, Beijing, 2006.

[6] W. J. Sun, Y. W. Wang, and X. K. Li, "Analysis on hydrogeological classification and water inrush accidents in North China coal mines," *Coal Engineering*, vol. 47, no. 6, pp. 103–105, 2015.

[7] C. C. Chu, "Study on the failure characteristics of the overburden strata induced by mining of underlying Ordovician limestone nappe aquifer," *Geological Journal of China Universities*, vol. 21, no. 3, pp. 569–576, 2015.

[8] C. C. Chu, "Investigation on the responses of overburden stress and water pressure to mining under the reverse fault," *Geofluids*, vol. 2021, Article ID 5199755, 11 pages, 2021.

[9] B. B. Yang, J. Liu, X. Zhao, and S. Zheng, "Evaporation and cracked soda soil improved by fly ash from recycled materials," *Land Degradation & Development*, vol. 32, no. 9, pp. 2823–2832, 2021.

[10] B. B. Yang, D. Li, S. Yuan, and L. Jin, "Role of biochar from corn straw in influencing crack propagation and evaporation in sodic soils," *Catena*, vol. 204, article 105457, 2021.

[11] B. B. Yang, S. Yuan, Y. Liang, and J. Liu, "Investigation of overburden failure characteristics due to combined mining: case study, Henan Province, China," *Environmental Earth Sciences*, vol. 80, no. 4, p. 143, 2021.

[12] B. X. Yuan, Z. H. Li, Z. Q. Zhao, H. Ni, Z. Su, and Z. Li, "Experimental study of displacement field of layered soils surrounding laterally loaded pile based on transparent soil," *Journal of Soils and Sediments*, vol. 21, no. 9, pp. 3072–3083, 2021.

[13] B. X. Yuan, Z. H. Li, Z. L. Su, Q. Luo, M. Chen, and Z. Zhao, "Sensitivity of multistage fill slope based on finite element model," *Advances in Civil Engineering*, vol. 2021, Article ID 6622936, 13 pages, 2021.

[14] B. X. Yuan, Z. H. Li, Y. Chen et al., "Mechanical and microstructural properties of recycling granite residual soil reinforced with glass fiber and liquid-modified polyvinyl alcohol polymer," *Chemosphere*, vol. 286, Part 1, 2022.

[15] L. Wang, X. M. Zeng, H. M. Yang et al., "Investigation and application of fractal theory in cement-based materials: a review," *Fractal and Fractional*, vol. 5, no. 4, p. 247, 2021.

[16] Z. Huang, K. Zhao, X. Z. Li, W. Zhong, and Y. Wu, "Numerical characterization of groundwater flow and fracture-induced water inrush in tunnels," *Tunnelling and Underground Space Technology*, vol. 116, article 104119, 2021.

[17] J. Huang, W. Li, D. Huang et al., "Fractal analysis on pore structure and hydration of magnesium oxysulfate cements by first principle, thermodynamic and microstructure-based methods," *Fractal and Fractional*, vol. 5, no. 4, p. 164, 2021.

[18] Z. Huang, Q. X. Gu, Y. F. Wu et al., "Effects of confining pressure on acoustic emission and failure characteristics of sandstone," *International Journal of Mining Science and Technology*, vol. 31, no. 5, pp. 963–974, 2021.

[19] Z. P. Meng, Y. F. Gao, A. H. Lu, R. Wang, X. Qiao, and C. Y. Huang, "Water inrush risk evaluation of coal mining under Quaternary alluvial water and reasonable design method of waterproof coal pillar," *Journal of Mining and Safety Engineering*, vol. 30, no. 1, pp. 23–29, 2013.

[20] B. B. Yang, K. Xu, and Z. Zhang, "Mitigating evaporation and desiccation cracks in soil with the sustainable material biochar," *Soil Science Society of America Journal*, vol. 84, no. 2, pp. 461–471, 2020.

[21] B. B. Yang and Y. Liu, "Application of fractals to evaluate fractures of rock due to mining," *Fractal and Fractional*, vol. 6, no. 2, p. 96, 2022.

[22] L. Wang, X. Lu, L. Liu et al., "Influence of MgO on the hydration and shrinkage behavior of low heat Portland cement-based materials via pore structural and fractal analysis," *Fractal and Fractional*, vol. 6, no. 1, p. 40, 2022.

[23] B. Yuan, M. Sun, L. Xiong, Q. Luo, S. P. Pradhan, and H. Li, "Investigation of 3D deformation of transparent soil around a laterally loaded pile based on a hydraulic gradient model

test," *Journal of Building Engineering*, vol. 28, no. 6, article 101024, 2020.

[24] L. W. Chen, H. R. Gui, and Y. F. Li, "UDEC simulation of the water2pouring probability in exploiting waterproof coal pillars under the conditions of thick loose bed and ultrathin overlying strata," *Hydrogeology & Engineering Geology*, vol. 1, pp. 53–56, 2007.

[25] W. H. Sui, G. T. Cai, and Q. H. Dong, "Experimental research on critical percolation gradient of quicksand across overburden fissures due to coal mining near unconsolidated soil layers," *Chinese Journal of Rock Mechanics and Engineering*, vol. 26, no. 10, pp. 2084–2091, 2007.

[26] J. L. Xu, D. Cai, and K. L. Fu, "Mechanism and prevention of working face pressure in adjacent unconsolidated confined aquifer," *Journal of China Coal Society*, vol. 32, no. 12, pp. 1239–1243, 2007.

[27] X. Z. Wang, *Occurrence condition and prevention technology of water inrush disaster of coal mining support under unconsolidated confined aquifer*, China University of Mining and Technology, Xuzhou, 2015.

[28] W. Wx, S. Wh, D. Qg, H. Ww, and G. Sx, "Closure effect of mining-induced fractures under sand aquifers and prediction of overburden failure due to re-mining," *Journal of China Coal Society*, vol. 38, no. 10, pp. 1728–1734, 2013.

[29] State Coal Industry Administration, *Procedures for Coal Pillar Reservation and Coal Mining of Buildings, Water Bodies, Railways and Main Roadways*, China Coal Industry Press, Beijing, 2017.

[30] L. Li, S. Li, X. Feng et al., "Numerical analysis and fluid-solid coupling model tests of coal mining under loose confined aquifer," *Chinese Journal of Geotechnical Engineering*, vol. 35, no. 4, pp. 679–690, 2013.

[31] W. H. Sui and Q. H. Dong, "Variation of pore water pressure and its precursor significance for quicksand disasters due to mining near unconsolidated formations," *Chinese Journal of Rock Mechanics and Engineering*, vol. 27, no. 9, pp. 1908–1916, 2008.

[32] W. G. Du, J. Chai, and D. D. Zhang, "Optical fiber sensing and characterization of water flowing fracture development in mining overburden," *Journal of China Coal Society*, vol. 46, no. 5, pp. 1565–1575, 2021.